CHALMERS

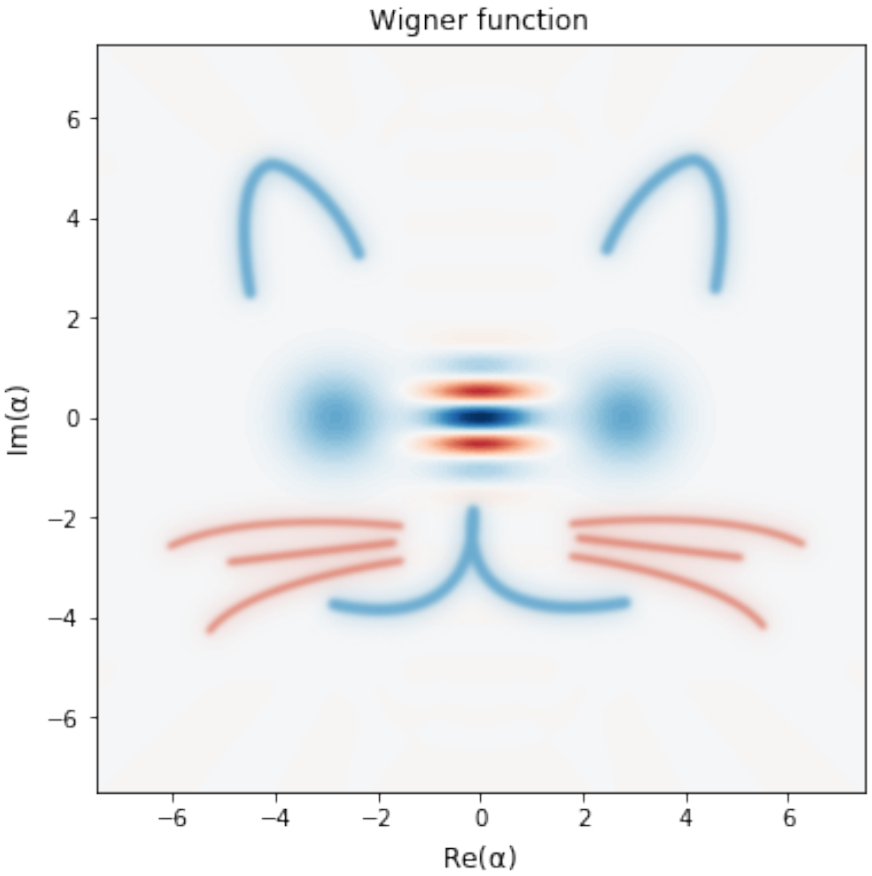

Cat State Preparation By Quantum Optimal Control with Krotov's Method

How to prepare your cat

Master's thesis in Quantum Computing

JOHAN WINTHER

Department of Microtechnology and Nanoscience
CHALMERS UNIVERSITY OF TECHNOLOGY
Göteborg, Sweden 2019

MASTER'S THESIS IN QUANTUM COMPUTING

Cat State Preparation By Quantum Optimal Control with Krotov's Method

How to prepare your cat

JOHAN WINTHER

Department of Microtechnology and Nanoscience
Division of Applied Quantum Mechanics
CHALMERS UNIVERSITY OF TECHNOLOGY

Göteborg, Sweden 2019

Cat State Preparation By Quantum Optimal Control with Krotov's Method
How to prepare your cat
JOHAN WINTHER

Master's thesis 2019:XX
ISSN 1652-8557
Department of Microtechnology and Nanoscience
Division of Applied Quantum Mechanics
Chalmers University of Technology
SE-412 96 Göteborg
Sweden
Telephone: +46 (0)31-772 1000

Cover:
Some explanation

Chalmers Reproservice
Göteborg, Sweden 2019

Cat State Preparation By Quantum Optimal Control with Krotov's Method
How to prepare your cat

JOHAN WINTHER
Department of Microtechnology and Nanoscience
Division of Applied Quantum Mechanics
Chalmers University of Technology

Abstract

Quantum computing has gained a lot of interest in recent years and commercial products are just now entering the market. However one of the main challenges in realising a quantum computer is noise and one key technology to remedy this is quantum error correction (QEC). One way of performing QEC is to store the quantum information of a qubit, while it's idle, as special basis states in a resonator. To do this one needs to apply encoding and decoding pulses to the coupled qubit-resonator system to do a state transfer. These pulses are hard or perhaps impossible to solve for analytically, which means they need to be numerically obtained by simulation.

This thesis studies the prospects of using Krotov's method (gradient ascent) to numerically optimize encoding pulses for state transfer. The Python package Krotov, a package for quantum optimal control using Krotov's method, is used to perform state transfers $|0\rangle$ to $|1\rangle$ and $|0\rangle$ to $|2\rangle$ of an anharmonic resonator. It is shown that, assuming a maximum drive amplitude and no dissipation, the method can realise a $|0\rangle$ to $|1\rangle$ transfer with fidelity $F > 0.99999$ with a total pulse length of only 10.75 ns. For the $|0\rangle$ to $|2\rangle$ transfer a total pulse length of 30 ns is needed to reach the same fidelity. Thus it is concluded that state transfers using Krotov for non-coupled systems is viable.

However for coupled systems there is great difficulty in using Krotov, as the package assumes a time-independent control Hamiltonian. A potential workaround for this problem is also presented.

Keywords: quantum computing, quantum optimal control, cat state, cat code

Sammanfattning

Preface

Acknowledgements

I would like to thank

Nomenclature

Lorem ipsum dolor sit amet, consectetuer adipiscing elit. Ut purus elit, vestibulum ut, placerat ac, adipiscing vitae, felis. Curabitur dictum gravida mauris. Nam arcu libero, nonummy eget, consectetuer id, vulputate a, magna. Donec vehicula augue eu neque. Pellentesque habitant morbi tristique senectus et netus et malesuada fames ac turpis egestas. Mauris ut leo. Cras viverra metus rhoncus sem. Nulla et lectus vestibulum urna fringilla ultrices. Phasellus eu tellus sit amet tortor gravida placerat. Integer sapien est, iaculis in, pretium quis, viverra ac, nunc. Praesent eget sem vel leo ultrices bibendum. Aenean faucibus. Morbi dolor nulla, malesuada eu, pulvinar at, mollis ac, nulla. Curabitur auctor semper nulla. Donec varius orci eget risus. Duis nibh mi, congue eu, accumsan eleifend, sagittis quis, diam. Duis eget orci sit amet orci dignissim rutrum.

Nam dui ligula, fringilla a, euismod sodales, sollicitudin vel, wisi. Morbi auctor lorem non justo. Nam lacus libero, pretium at, lobortis vitae, ultricies et, tellus. Donec aliquet, tortor sed accumsan bibendum, erat ligula aliquet magna, vitae ornare odio metus a mi. Morbi ac orci et nisl hendrerit mollis. Suspendisse ut massa. Cras nec ante. Pellentesque a nulla. Cum sociis natoque penatibus et magnis dis parturient montes, nascetur ridiculus mus. Aliquam tincidunt urna. Nulla ullamcorper vestibulum turpis. Pellentesque cursus luctus mauris.

Nulla malesuada porttitor diam. Donec felis erat, congue non, volutpat at, tincidunt tristique, libero. Vivamus viverra fermentum felis. Donec nonummy pellentesque ante. Phasellus adipiscing semper elit. Proin fermentum massa ac quam. Sed diam turpis, molestie vitae, placerat a, molestie nec, leo. Maecenas lacinia. Nam ipsum ligula, eleifend at, accumsan nec, suscipit a, ipsum. Morbi blandit ligula feugiat magna. Nunc eleifend consequat lorem. Sed lacinia nulla vitae enim. Pellentesque tincidunt purus vel magna. Integer non enim. Praesent euismod nunc eu purus. Donec bibendum quam in tellus. Nullam cursus pulvinar lectus. Donec et mi. Nam vulputate metus eu enim. Vestibulum pellentesque felis eu massa.

Contents

1 Introduction

Quantum computing is starting to appear in commercial products [1], however, despite a lot of progress [2], there are still a lot of challenges to be solved before large scale quantum computers become commonplace. Unlike classical computers, where the transistors' on and off state is dictated by the stream of many electrons, quantum computers rely on single or very few number of particles which make the quantum states very delicate [3].

One of the key technologies to keep these states in quantum computing is quantum error correction (QEC) [3], which is a way to retain the quantum information in a qubit by introducing redundancy into the physical system. Leghtas, Kirchmair, Vlastakis, *et al.* [4], Mirrahimi, Leghtas, Albert, *et al.* [5] propose and Ofek, Petrenko, Heeres, *et al.* [6] demonstrate a method to encode the quantum information in a clever basis in quantum harmonic resonators.

To further clarify, in this scheme the quantum information of a qubit is carefully encoded and decoded into a resonator by applying optimized microwave pulses to the qubit and resonator system which will realise state transfers in both these systems. This thesis will focus on how to numerically optimize encoding and decoding pulses using Krotov's method [7], a gradient ascent based optimization algorithm available publicly as a ready-to-use Python package [8].

1.1 Purpose

The purpose of this thesis is to numerically optimize microwave pulses to transfer the quantum information in a qubit to a resonator. This will be done using the Krotov Python package [8].

1.2 Limitations of the thesis

In this thesis, the limitations will be the following:

- The quantum systems are assumed to be closed systems without any interaction with the environment.
- The step size in Krotov's method will be constant throughout the optimizations.
- Single optimization goal (although multiple simultaneous are possible).

2 Theory

In this chapter the theoretical concepts will be explained. However it is assumed that the reader has a basic understanding of quantum mechanics.

2.1 Superconducting resonators

Superconducting resonators are used in quantum computing both as the basis for qubits and as readout and control components. Although ideal resonators have equally spaced energy levels, in reality they are more or less anharmonic and the general Hamiltonian for a quantum anharmonic resonator is

$$\hat{H} = \omega \hat{a}^\dagger \hat{a} + \frac{\kappa}{2}\left(\hat{a}^\dagger \hat{a}\right)^2 \tag{2.1}$$

where ω is the resonance frequency, κ is the anharmonic (self-Kerr) term and $\hat{a}$ is the destruction operator which removes an excitation from the resonator. Note that this is still an approximation as higher order terms have been neglected.

The anharmonicity can be vizualised, see fig. 2.1, by plotting the eigenenergies of eq. (2.1) as a function of κ. A larger (negative) anharmonicity makes the energy spacing smaller for higher excitation states. This anharmonicity is what permits a resonator to act as a qubit, as it is possible to adress only the first two states $|0\rangle$ and $|1\rangle$. Throughout this thesis, a qubit will be used to refer to an anharmonic resonator even though it has more than two energy levels. Further, the energy spacing between states $|i\rangle$ and $|j\rangle$ will be referred to as ω_{ij} and the "resonance frequency of the qubit" as ω_{01}.

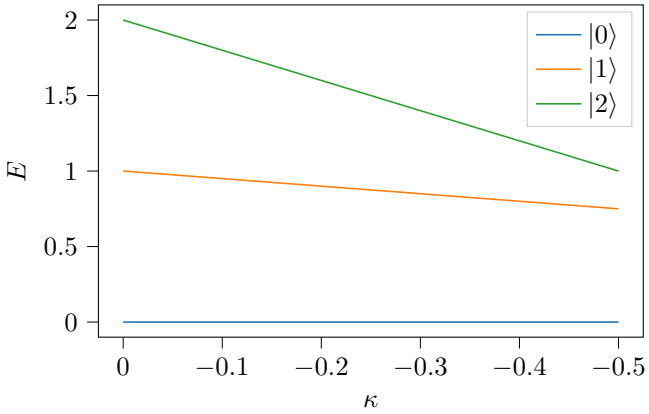

Figure 2.1: The energy levels of a three-level resonator for anharmonicity $\kappa \in [-0.5, 0]$ and $\omega = 1$. Note that the x-axis is reversed.

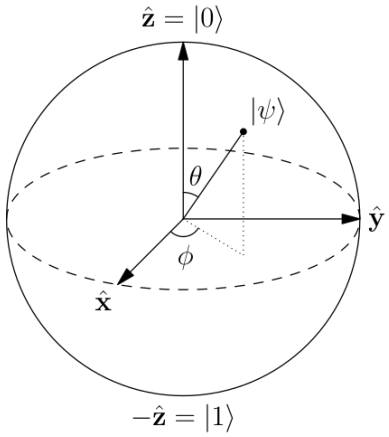

Figure 2.2: Representation of an abritrary pure quantum state on the Bloch sphere.
Source: [9] (CC BY-SA 3.0).

2.2 Coupled Qubit Cavity System

The Hamiltonian for a coupled qubit and resonator is chosen as

$$\hat{H}(t) = \underbrace{\omega_r \hat{a}^\dagger \hat{a} + \frac{\kappa_r}{2}\left(\hat{a}^\dagger \hat{a}\right)^2}_{\text{Resonator}} + \underbrace{\omega_{01} \hat{b}^\dagger \hat{b} + \frac{\kappa_q}{2}\left(\hat{b}^\dagger \hat{b}\right)^2}_{\text{Qubit}} + \underbrace{g\left(\hat{a}^\dagger \hat{b} + \hat{a}\hat{b}^\dagger\right)}_{\text{Coupling}} \tag{2.2}$$

where $\hat{b}$ is the destruction operator for the qubit. There is now a coupling term with the coupling strength g.

2.3 Visualization of quantum states

In order to understand the results presented later in this thesis, some visualization techniques of quantum states are shown and explained.

2.3.1 Bloch sphere

The pure state of a qubit can be visualized on the surface of a unit sphere with the following parametrization

$$|\psi\rangle = \cos\left(\frac{\theta}{2}\right)|0\rangle + \mathrm{e}^{i\phi}\sin\left(\frac{\theta}{2}\right)|1\rangle \tag{2.3}$$

where θ and ϕ are angles which are shown in fig. 2.2. The ground state $|0\rangle$ is located on the "north pole" and the excited state $|1\rangle$ on the "south pole".

2.3.2 Density matrices and Hinton diagrams

2.3.3 Wigner function

2.4 Bosonic codes

2.4.1 Cat codes

2.5 Quantum optimal control

Quantum control is the process of controlling a quantum system by controlling the amplitude of a set of control operators in time [10]. Such a system can be described [10] by a Hamiltonian of the following form

$$\hat{H}(t) = \underbrace{\hat{H}_d}_{\text{Drift}} + \underbrace{u_0(t)\hat{H}_0 + \ldots + u_N(t)\hat{H}_N}_{\text{Control}}. \tag{2.4}$$

The controls are usually electromagnetic pulses changing in time and thus will be referred to as "pulse shapes" [10] in this thesis .

There are two main questions in quantum control: one of *controllability* and one of *optimal control*. The first deals with the *existence* of solutions given a Hamiltonian and the second with the *optimized* solutions for the pulse shapes $\{u_i(t)\}$ [11]. The optimal solutions are generally not analytically solvable and thus the pulse shapes need to be discretized in time and numerically optimized using algorithms. The algorithm used for this thesis is called Krotov's method and will be presented in the Method chapter.

2.5.1 Unitary transformation

A unitary transformation can significantly simplify systems that are hard to simulate. This idea will be conceptually presented here and then implemented in the Method chapter. The unitary transformation that is used is a special case of transformations called the *interaction picture* where the Hamiltonian is split up into a time-independent and time-dependent part

$$\hat{H}(t) = \hat{H}_A + \hat{H}_B(t). \tag{2.5}$$

By choosing the unitary operator $\hat{U} = \mathrm{e}^{i\hat{H}_A t}$ the unitary transformation takes us into the interaction picture

$$\begin{aligned}
\hat{H} \rightarrow\ & \hat{U}\Big[\hat{H}_A + \hat{H}_B(t)\Big]\hat{U}^\dagger + i\frac{\mathrm{d}\hat{U}}{\mathrm{d}t}\hat{U}^\dagger = \\
=\ & \hat{U}\hat{H}_A\hat{U}^\dagger + \hat{U}\hat{H}_B\hat{U}^\dagger + i\Big(i\hat{H}_A t\Big)\mathrm{e}^{i\hat{H}_A t}\mathrm{e}^{-i\hat{H}_A t} = \\
=\ & \hat{H}_A + \hat{U}\hat{H}_B\hat{U}^\dagger - \hat{H}_A = \hat{U}\hat{H}_B\hat{U}^\dagger
\end{aligned}$$

3 Method

In this chapter Krotov's method for quantum optimal control will be briefly introduced and an implementation as a Python package. Then the numerical experiments will be explained.

3.1 Krotov's Method for quantum optimal control

Krotov's method fundamentally relies on the variational principle to minimize a functional

$$J\Big[\Big\{\Big|\phi_k^{(i)}(t)\Big\rangle\Big\}, \Big\{\epsilon_l^{(i)}(t)\Big\}\Big]$$

where the constraints are included as Lagrange multipliers [8]. A detailed explanation of this functional when the method is applied to quantum systems can be found in [7].

The underlying principles of the Krotov's method will not be adressed in the thesis. Thus the method will be treated as a black box function provided by the Python package which will be presented in the next section.

3.1.1 Krotov: the Python package

A Python implementation of the Krotov's method is available at [8] which provides an abstraction layer for doing optimizations. The reason this package was chosen is primarily because it allows for optimization of multiple objectives. This is necessary in order to create a single encoding pulse which will realise the state transfer into the cat code basis for any arbitrary state.

It is built on top of QuTiP, a popular software package for simulating the dynamics of quantum systems [12].

3.2 Optimization Experiments

In this chapter the numerical optimization experiments are presented and motivated.

3.2.1 Hamiltonian

To test the method, the anharmonic oscillator in eq. (2.1) will be chosen as it is often used as the physical realisation of a qubit. Throughout this thesis, such a system will be referred to as a qubit even though it has more than two energy levels. Consequently, the resonance frequency of the qubit ω_{01} refers to the transition between $|0\rangle$ and $|1\rangle$. To induce transitions between these states, control pulse terms are added to eq. (2.1)

$$\hat{H} = \omega_{01}\hat{a}^\dagger\hat{a} + \frac{\kappa}{2}\big(\hat{a}^\dagger\hat{a}\big)^2 + \Omega(t)\mathrm{e}^{i\omega_{01}t}\hat{a} + \Omega^*(t)\mathrm{e}^{-i\omega_{01}t}\hat{a}^\dagger \tag{3.1}$$

where $\Omega(t)$ is the complex amplitude of the control pulse. Looking at the Hamiltonian above it can be argued that it can be written in the form in eq. (2.4) with $u_0(t) = \Omega(t)\mathrm{e}^{i\omega_{01}t}$ and $u_1(t) = \Omega^*(t)\mathrm{e}^{-i\omega_{01}t}$. However, there are two problems that need to be adressed. Firstly, the oscillating factors will require an unnecessarily fine time discretization of the pulses. Secondly, the Krotov package expects real-valued pulse amplitudes $\{u_i(t)\}$ as inputs. The first problem can be avoided by transforming the Hamiltonian into the interaction picture. Choosing $H_A = \omega_{01}\hat{a}^\dagger\hat{a}$, eq. (3.1) transforms[1] into

$$\hat{H} \rightarrow \ \frac{\kappa}{2}\big(\hat{a}^\dagger\hat{a}\big)^2 + \Omega(t)\hat{a} + \Omega^*(t)\hat{a}^\dagger. \tag{3.2}$$

Now the pulse amplitudes are $u_0(t) = \Omega(t)$ and $u_1(t) = \Omega^*(t)$, i.e. the envelope of the physical control pulse which varies significantly slower than the actual pulse. The second problem can now be easily fixed with a rearrangment of the terms

$$\Omega(t)\hat{a} + \Omega^*(t)\hat{a}^\dagger = \Big[\mathrm{Re}[\Omega(t)] + i\mathrm{Im}[\Omega(t)]\Big]\hat{a} + \Big[\mathrm{Re}[\Omega(t)] - i\mathrm{Im}[\Omega(t)]\Big]\hat{a}^\dagger =$$

$$= \mathrm{Re}[\Omega(t)]\big(\hat{a} + \hat{a}^\dagger\big) + \mathrm{Im}[\Omega(t)]i\big(\hat{a} - \hat{a}^\dagger\big).$$

For intuition, $\big(\hat{a} + \hat{a}^\dagger\big)$ and $i\big(\hat{a} - \hat{a}^\dagger\big)$ correspond to Bloch sphere rotations around the x-axis and y-axis respectively. This leaves us with the final Hamiltonian

$$\hat{H} = \underbrace{\kappa/2\big(\hat{a}^\dagger\hat{a}\big)^2}_{\hat{H}_d} + \underbrace{\mathrm{Re}[\Omega(t)]}_{u_0(t)}\underbrace{(\hat{a} + \hat{a}^\dagger)}_{\hat{H}_0} + \underbrace{\mathrm{Im}[\Omega(t)]}_{u_1(t)}\underbrace{i(\hat{a} - \hat{a}^\dagger)}_{\hat{H}_1}. \tag{3.3}$$

The parameters of the qubit are chosen to model real superconducting qubits with $\kappa = -2\pi \times 297\,\mathrm{MHz}$ (and $\omega_{01} = 2\pi \times 6.2815\,\mathrm{GHz}$). The system Hamiltonian (3.3) is simulated with a Hilbert space size conveniently chosen to be $L = 3$. A smaller Hilbert space, and consequently smaller matrices, requires less computations but could possibly be a poor approximation of the Hamiltonian. This, however, is not a problem in this case as we can neglect

[1] Full derivation is shown in **??**

3.2.2 Optimization Setup

The goal of the optimization is to realise state transfers which will be presented in their own respective sections below. However the common setup options will be presented here.

To simulate the constraints of physical **a**rbitrary **w**aveform **g**enerators a maximum sample rate of $4\,\mathrm{GSa\,s^{-1}}$ is added. Recall that the physcal pulses oscillate at $\omega_{01} = 6.2815\,\mathrm{GHz}$, a rate which $4\,\mathrm{GSa\,s^{-1}}$ can never resolve. AWGs with higher sample rates than $4\,\mathrm{GSa\,s^{-1}}$ are costly, but the rotating frame transformation permits the use of an AWG to generate the pulse envelopes $\Omega(t)$ and a tone generator to create a carrier signal at ω_{01}. These signals can then be combined in a mixer. Thus the generated pulses can (eventually) be used in experimental settings. Further, due to the noise sensitivity of superconducting systems an amplitude constraint is needed to keep the system cool. Some derivation is required to set a realistic maximum amplitude A_m. First the maximum amplitude is chosen with the assumption that a truncated gaussian pulse

$$g(t) = \frac{1}{\sigma\sqrt{2\pi}} \mathrm{e}^{-\frac{1}{2}\left(\frac{t}{\sigma}\right)^2} \tag{3.4}$$

with $\sigma = 3\,\mathrm{ns}$ can physically realise a π-rotation $|0\rangle \to |1\rangle$ in a planar transmon qubit.

Krotov gives a Blackman pulse Blackman pulses are a window function A Blackman pulse with a total length of 6σ is a good approximation of a Gaussian pulse.

$$A(\sigma) = \frac{C}{\max(\sigma, 3)\sqrt{2\pi}} \tag{3.5}$$

we can use this to determine the maximum amplitude and

Guess pulses half amplitude (actually blackman pulses)

convergence criteria fidelity F change between iterations falls below a certain critera ΔF

3.2.3 $|0\rangle \to |1\rangle$ state transfer

Pulse shapes were optimized with varying lengths from 4.25 ns to 30 ns with convergence criteria $F > 0.99999$ or $\Delta F < 10^{-7}$. Step size $\lambda = \frac{1}{\frac{1}{2}A_m}$

3.2.4 $|0\rangle \to |2\rangle$ state transfer

Pulse shapes were optimized with varying lengths from 22 ns to 30 ns with convergence criteria $F > 0.99999$ or $\Delta F < 10^{-9}$. Step size $\lambda = \frac{1}{2A_m}$

3.2.5 $|1\rangle_q |0\rangle_r \to |0\rangle_q |C_1\rangle_r$ state transfer

Start with maximum pulse amplitude

4 Results

The results of the numerical experiments will be presented in this chapter. For both optimization targets the optimized pulses, their properties and the final evolved state will be presented.

4.1 $|0\rangle \to |1\rangle$ state transfer

In fig. 4.1 the fidelity during all optimization runs are plotted. For pulse lengths longer than 15 ns the fidelity starts at values close to the goal ($F > 0.9$) and the number of iterations is relatively low (less than 85 iterations). In contrast, pulses shorter than 15 ns start at lower fidelities while the number of iterations are roughly one order of magnitude larger with no clear pattern.

To give a more detailed picture, the starting fidelity and optimized fidelity is plotted over pulse length in fig. 4.2. The optimizations where the fidelity goal was not reached, pulse lengths equal to and below 10.50 ns, are marked with stars.

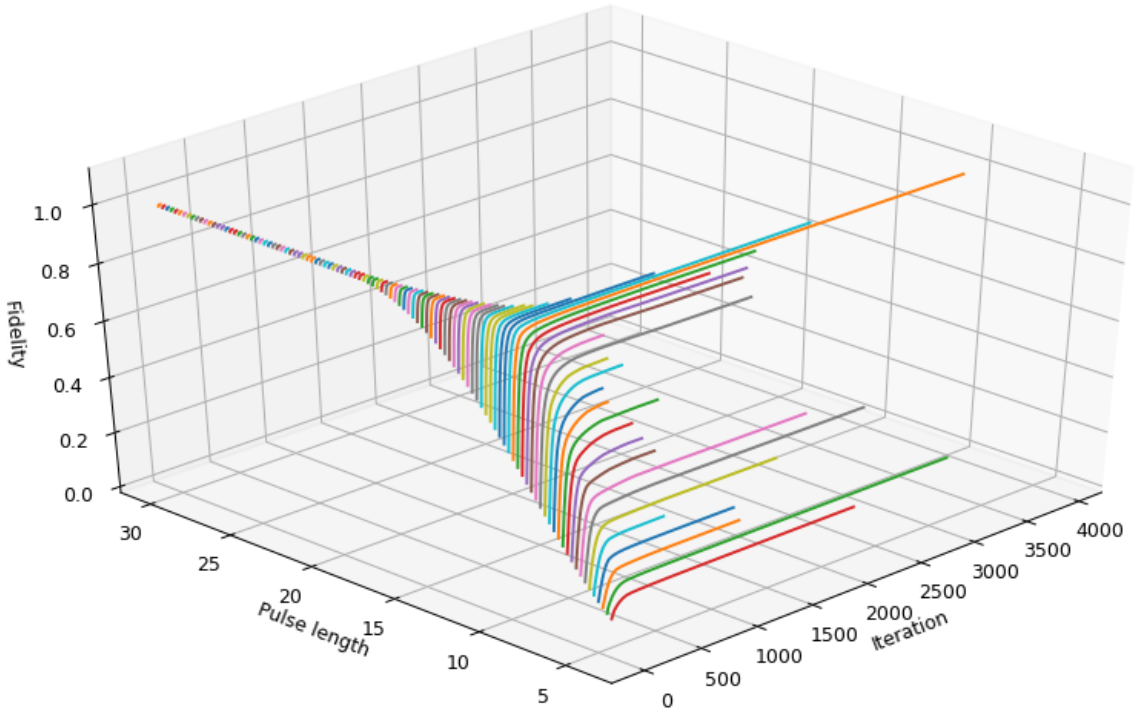

Figure 4.1: Fidelity during optimizations for every pulse length (ns). The different colors help distinguish the lines.

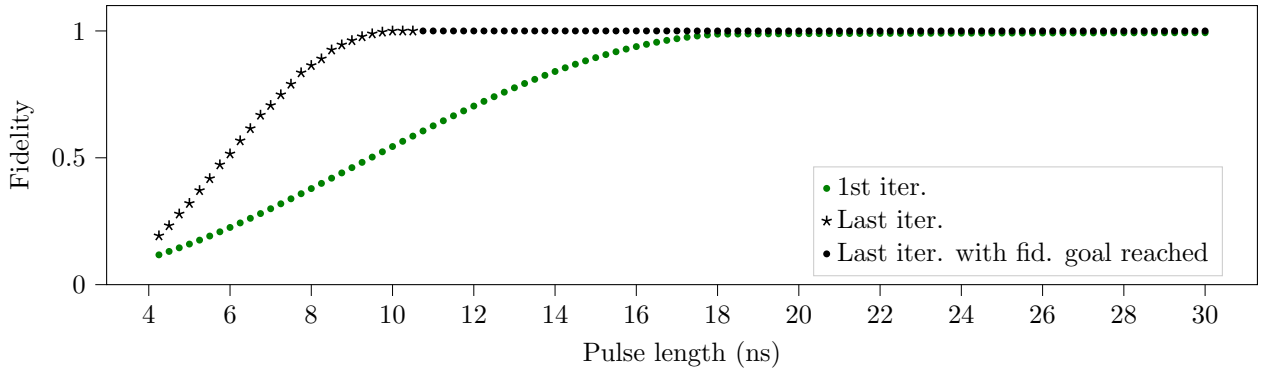

Figure 4.2: Fidelity of first and last iteration of every pulse length. The stable region above

Further analysis is done on pulses with lengths 4.25 ns, 6.0 ns, 8.0 ns, 10.0 ns, 20.0 ns and 30.0 ns. The optimized pulse shapes $\mathrm{Re}(\Omega)$ and $\mathrm{Im}(\Omega)$ are plotted in fig. 4.3 together with the guess pulses. Pulses longer than 20 ns require only fine adjustments to the Blackman guess pulse while shorter pulses have an imaginary part which is maximized for the whole duration of the pulse.

The spectrum of $\Omega(t)$ in the lab frame ($\Omega(t)e^{i\omega_{01}t}$) is shown in fig. 4.4. For all pulse lengths there is a peak centered roughly at ω_{01} and the width of the peak becomes narrower for longer pulses. For the highest pulse length 30 ns there is almost no support at ω_{02} and ω_{12}.

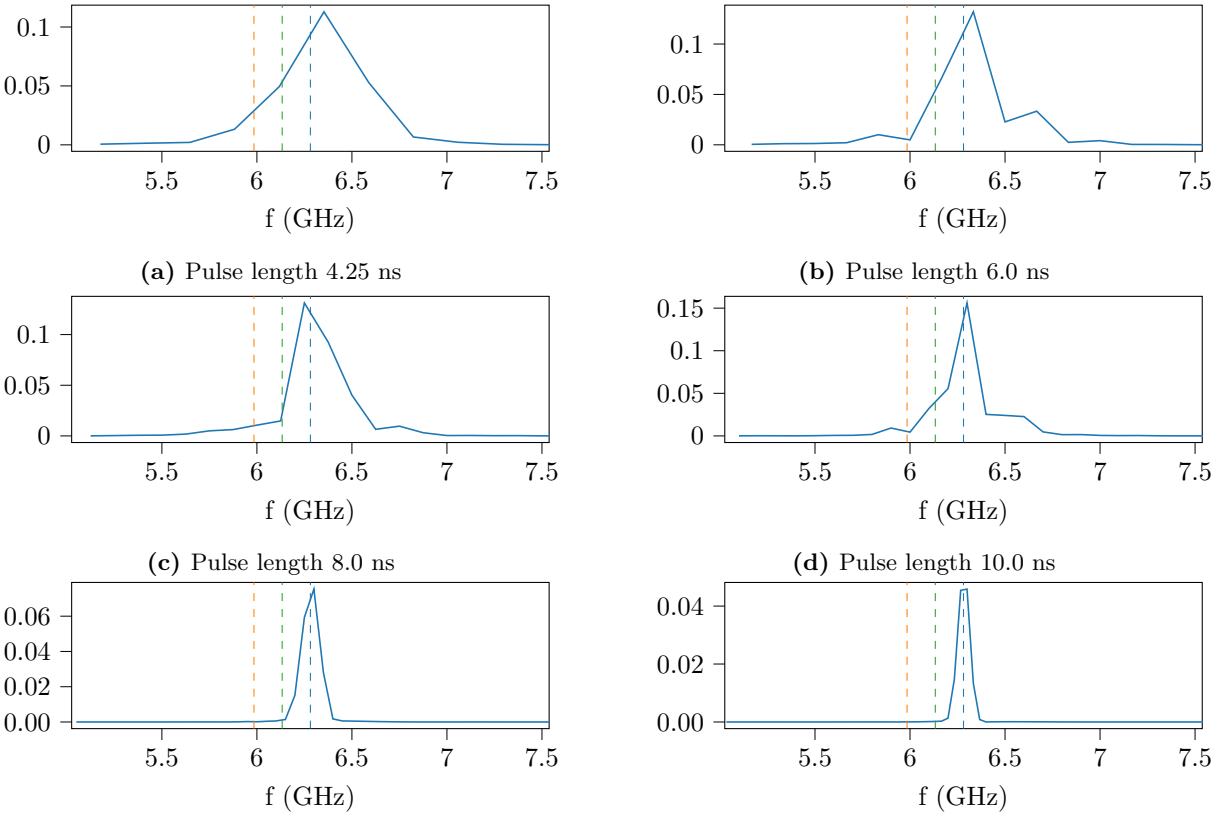

(a) Pulse length 4.25 ns

(b) Pulse length 6.0 ns

(c) Pulse length 8.0 ns

(d) Pulse length 10.0 ns

(e) Pulse length 20.0 ns

(f) Pulse length 30.0 ns

Figure 4.4: Pulse spectrum of the complex pulses in fig. 4.3. The vertical lines indicate (from left to right) ω_{02}, ω_{12}, ω_{01}.

The time evolution of the system under the optimized pulses are visualized by plotting the occupation of the states over time, fig. 4.5, the projection of the state on the Bloch sphere over time, fig. 4.6, and a Hinton diagram of the evolved final state, fig. 4.7.

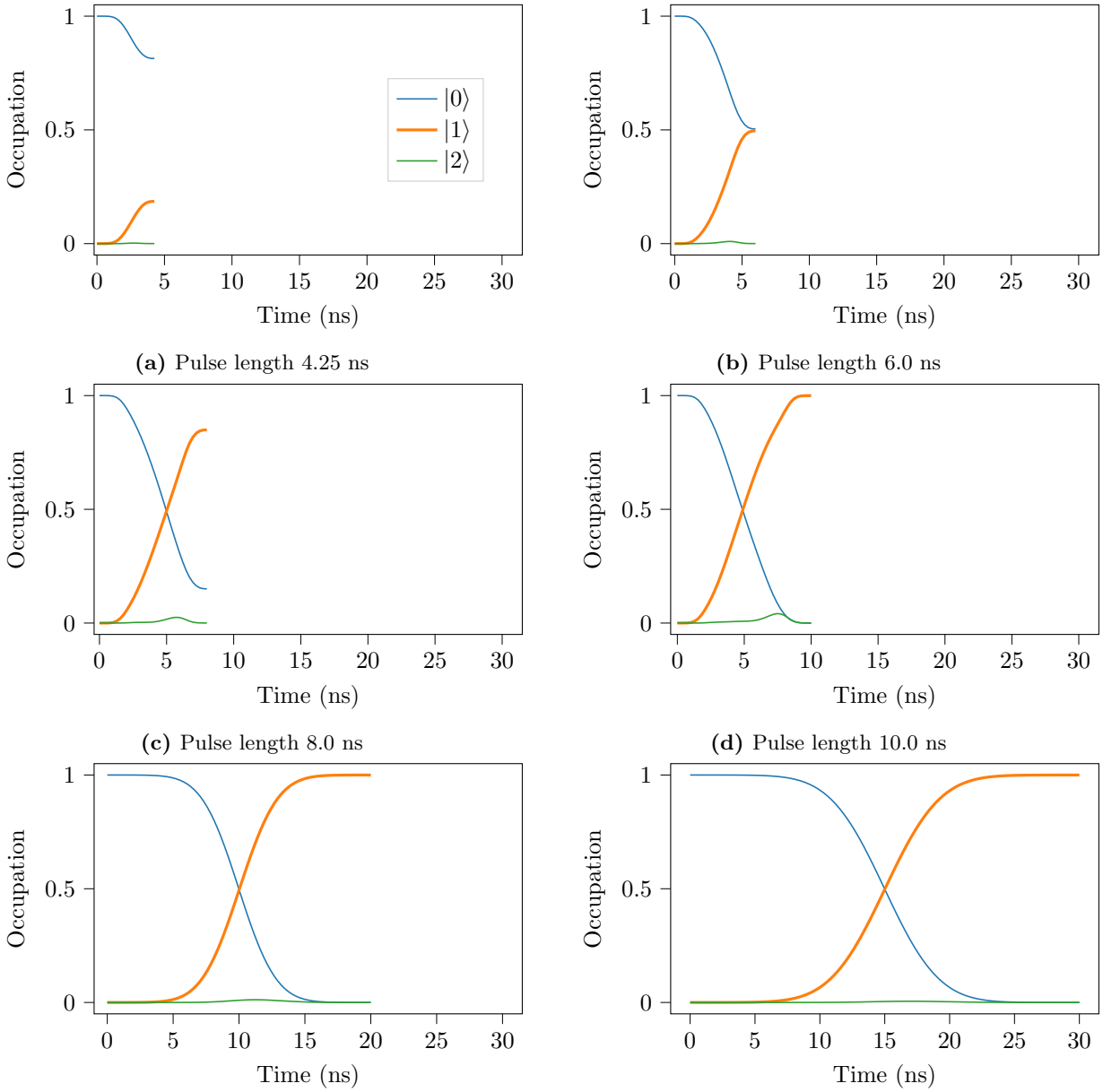

(a) Pulse length 4.25 ns

(b) Pulse length 6.0 ns

(c) Pulse length 8.0 ns

(d) Pulse length 10.0 ns

(e) Pulse length 20.0 ns

(f) Pulse length 30.0 ns

Figure 4.5: Energy level occupation over time for different lengths of optimized pulses.

For short pulse lengths there is not enough time for the transfer from $|0\rangle$ to $|1\rangle$, but for a pulse length of roughly 10.0 ns the goal is reached. Figure 4.5 **(b)** shows a little rise in occupation of $|2\rangle$ around 7.5 ns.

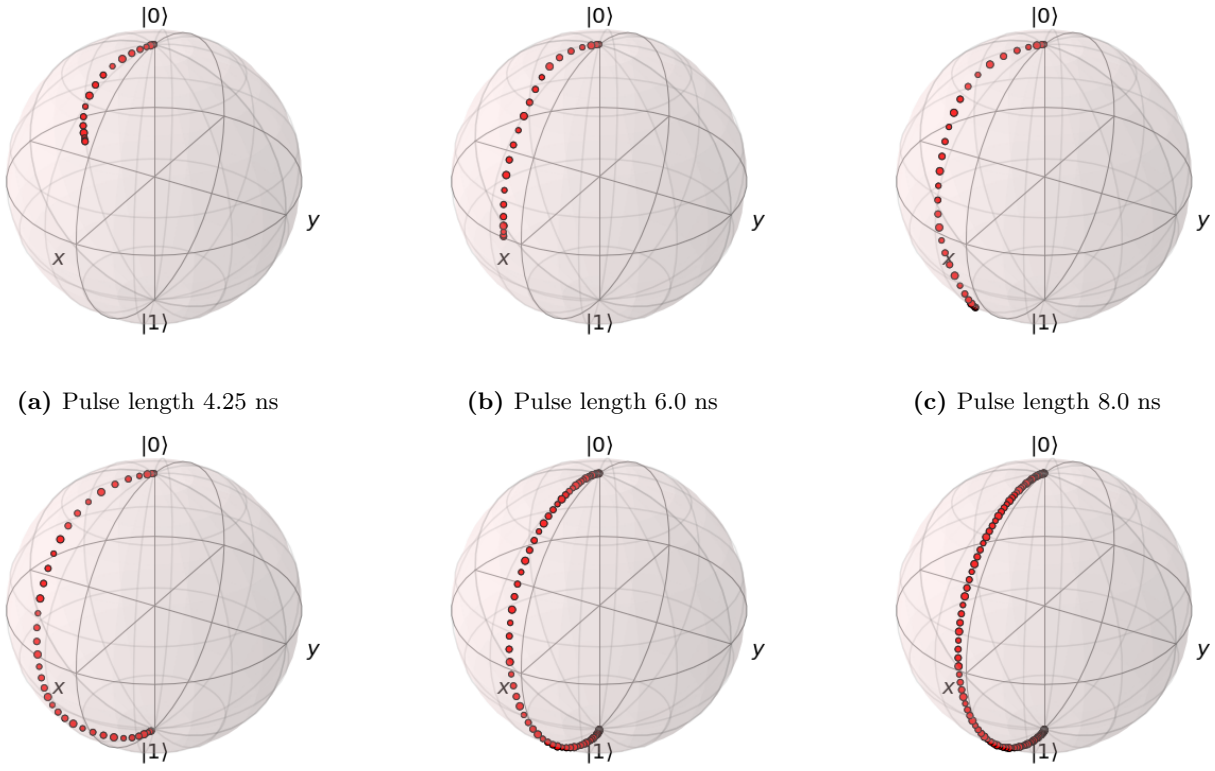

(a) Pulse length 4.25 ns **(b)** Pulse length 6.0 ns **(c)** Pulse length 8.0 ns

(d) Pulse length 10.0 ns **(e)** Pulse length 20.0 ns **(f)** Pulse length 30.0 ns

Figure 4.6: Time dynamics on the Bloch sphere for different lengths of optimized pulses.

Looking at fig. 4.6 we see that the transfer occurs along the y-axis for longer pulses.

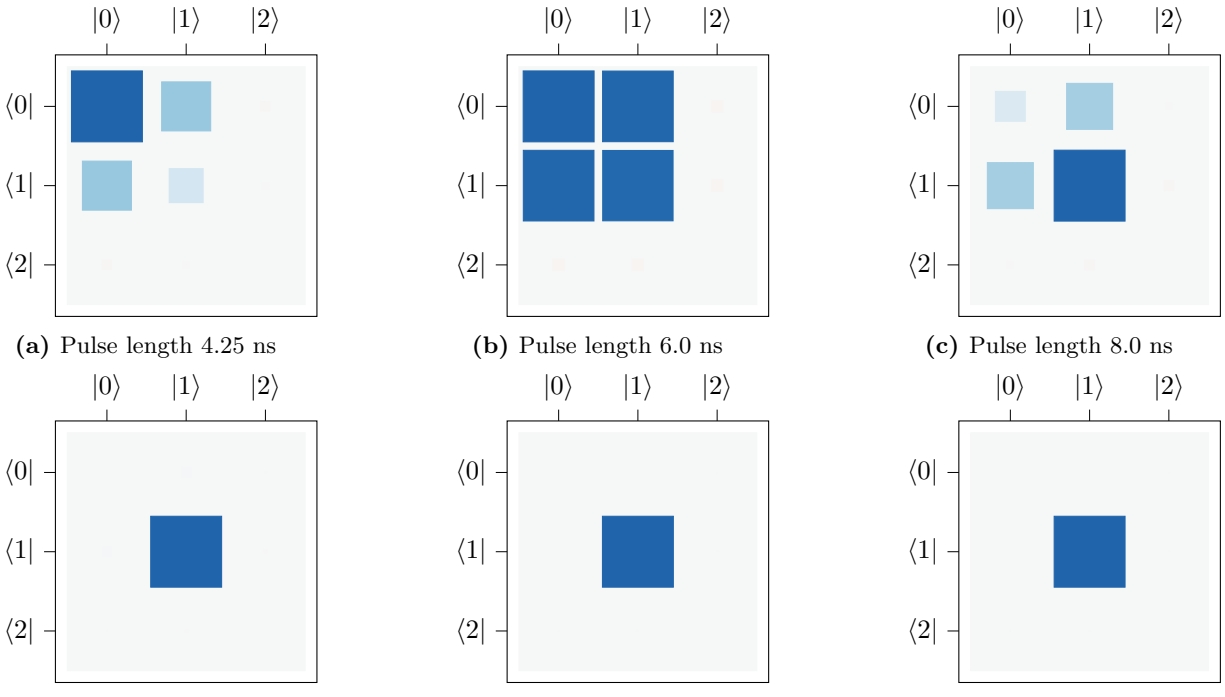

(a) Pulse length 4.25 ns **(b)** Pulse length 6.0 ns **(c)** Pulse length 8.0 ns

(d) Pulse length 10.0 ns **(e)** Pulse length 20.0 ns **(f)** Pulse length 30.0 ns

Figure 4.7: Hinton diagram of $|\psi(T)\rangle\langle\psi(T)|$

The Hinton diagram in fig. 4.7 provides a visualization of the density matrix $|\psi(T)\rangle\langle\psi(T)|$. The final density matrix shows how the much of the state is in the

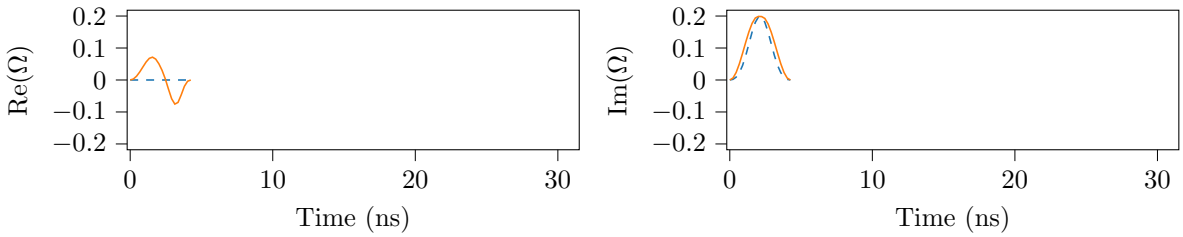

(a) Pulse length 4.25 ns

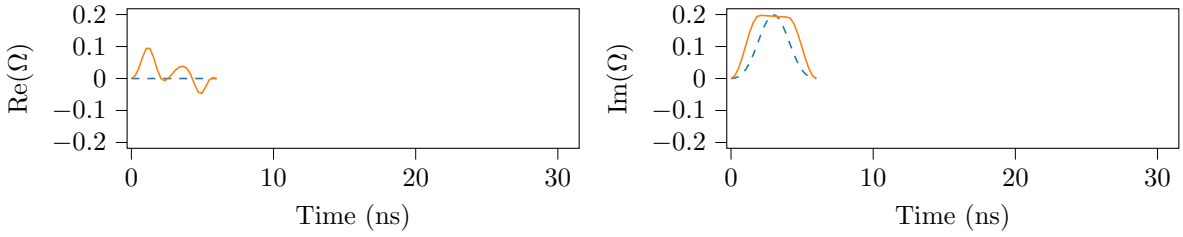

(b) Pulse length 6.0 ns

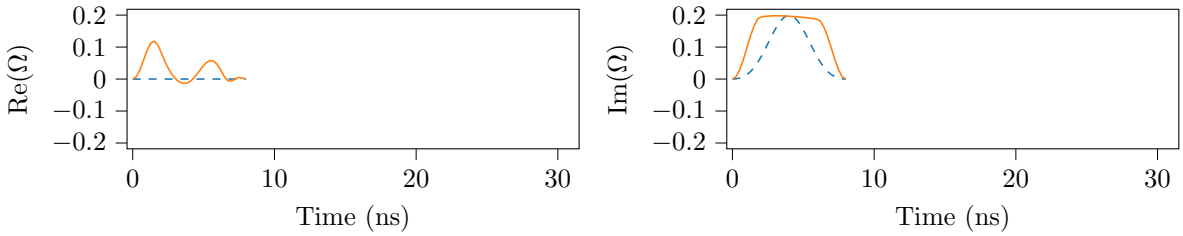

(c) Pulse length 8.0 ns

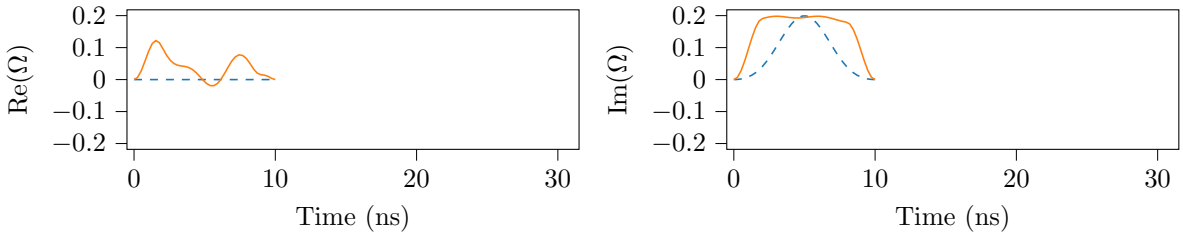

(d) Pulse length 10.0 ns

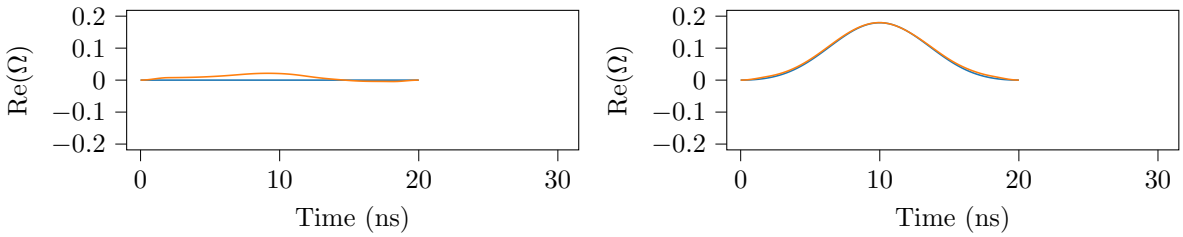

(e) Pulse length 20.0 ns

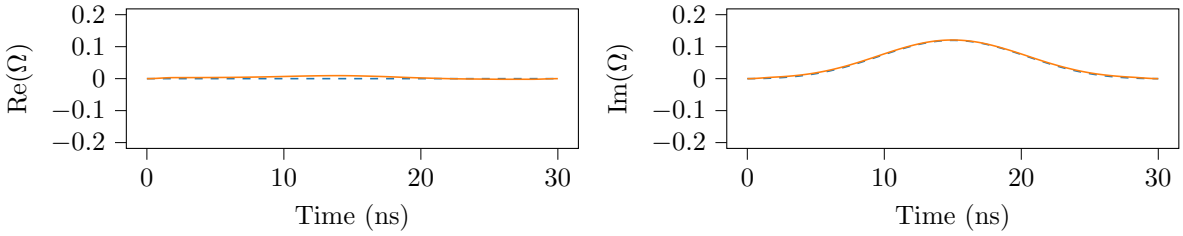

(f) Pulse length 30.0 ns

Figure 4.3: Optimised pulse shapes and guess pulses for pulse lengths **(a)** 4.25 ns, **(b)** 6.0 ns, **(c)** 8.0 ns, **(d)** 10.0 ns, **(e)** 20.0 ns, and **(f)** 30.0 ns. Short pulses (<10 ns) change substantially from the starting Blackman shape while long pulses (>20 ns) only require fine adjustments.

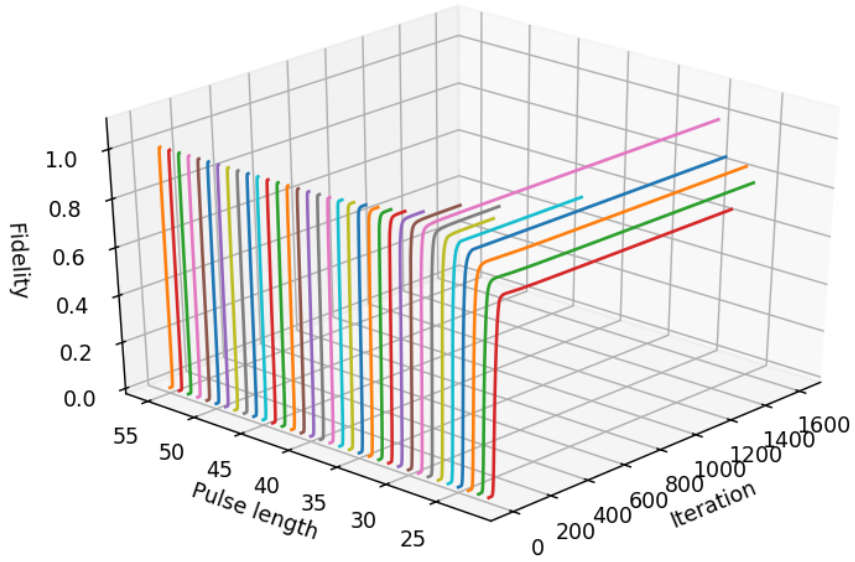

Figure 4.8: Fidelity during optimizations for every pulse length (ns).

4.2 $|0\rangle \rightarrow |2\rangle$ state transfer

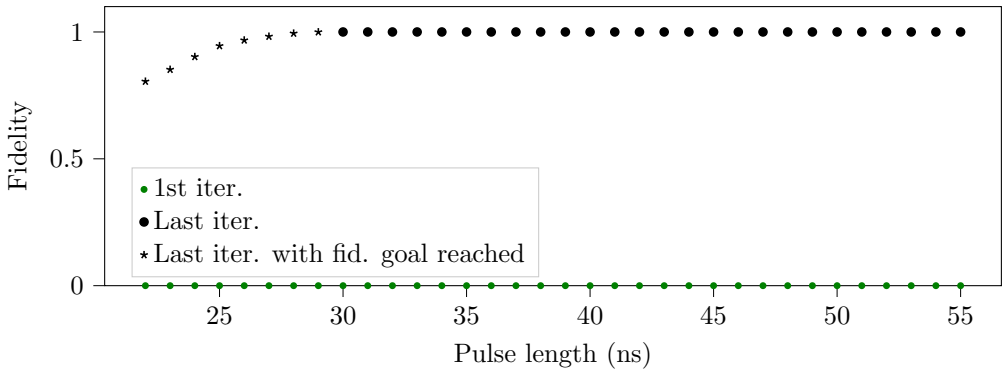

Figure 4.9: Fidelity of first and last iteration of every pulse length.

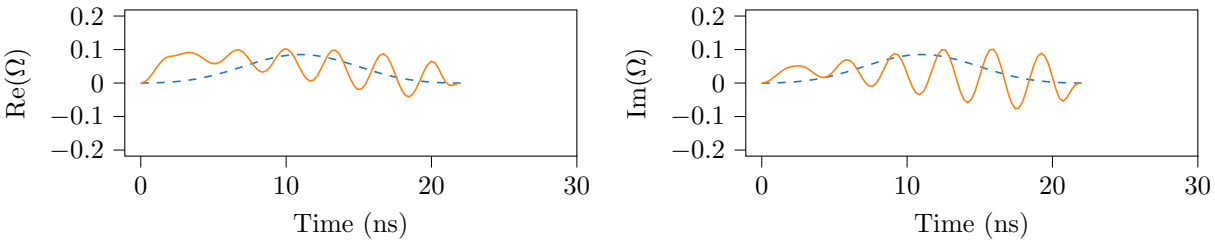

(a) Pulse length 22.0 ns

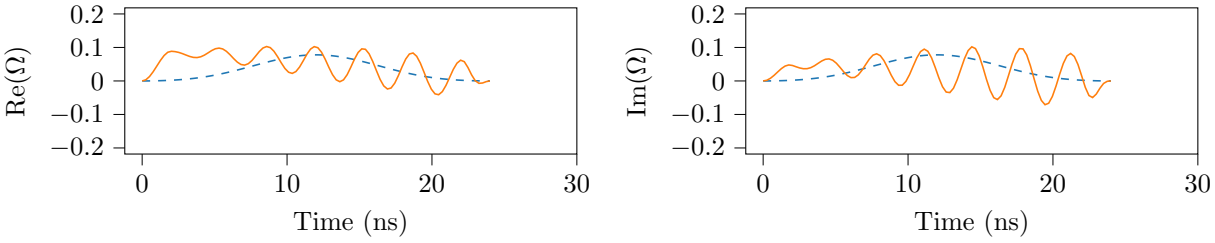

(b) Pulse length 24.0 ns

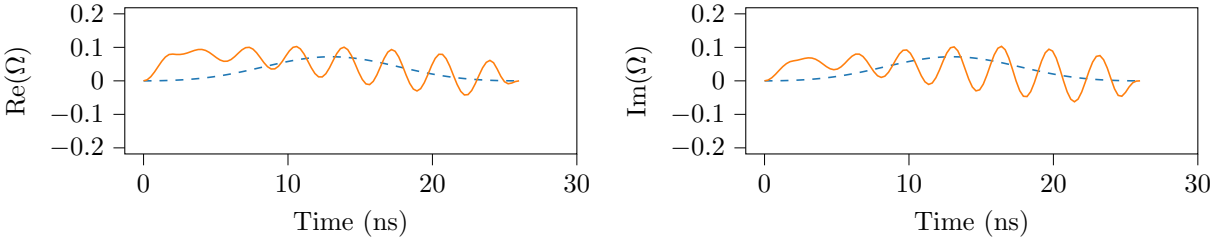

(c) Pulse length 26.0 ns

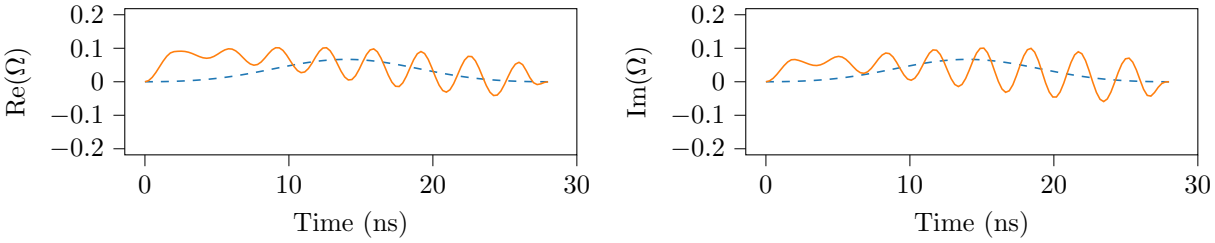

(d) Pulse length 28.0 ns

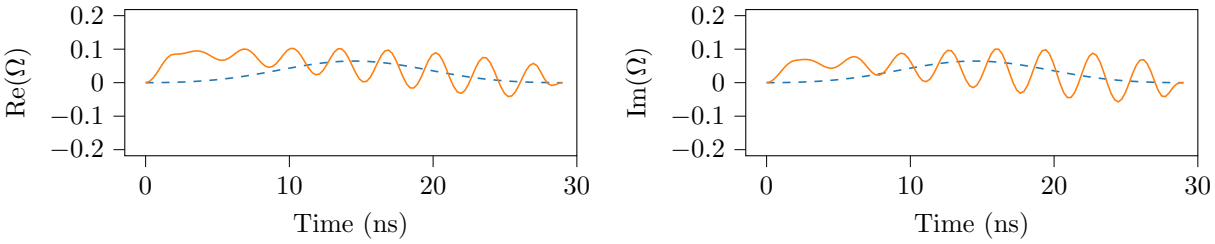

(e) Pulse length 29.0 ns

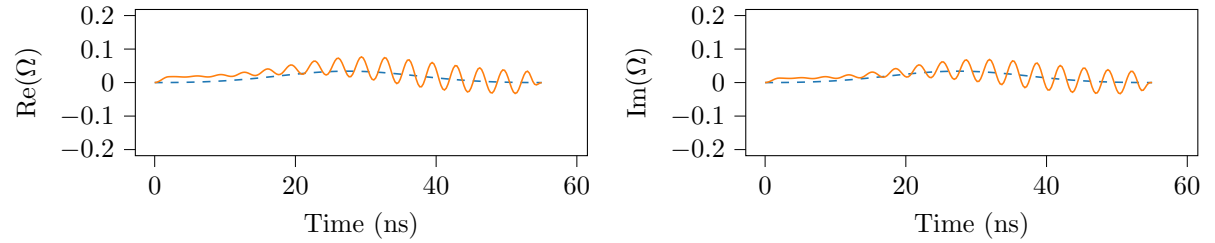

(f) Pulse length 55.0 ns

Figure 4.10: Pulse shapes.

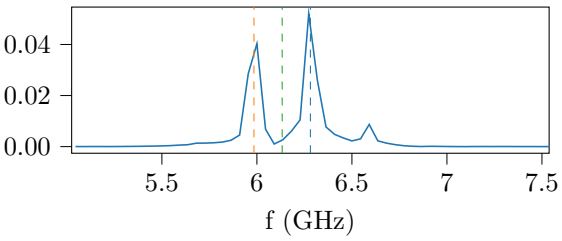

(a) Pulse length 22.0 ns

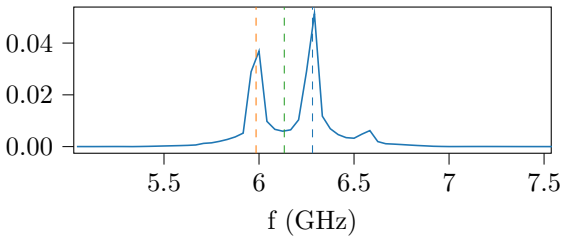

(b) Pulse length 24.0 ns

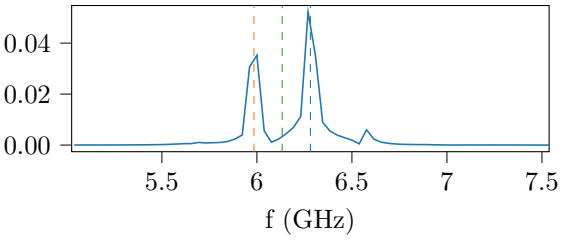

(c) Pulse length 26.0 ns

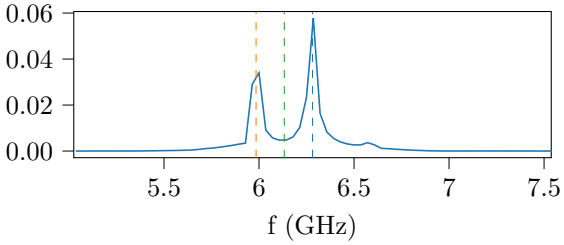

(d) Pulse length 28.0 ns

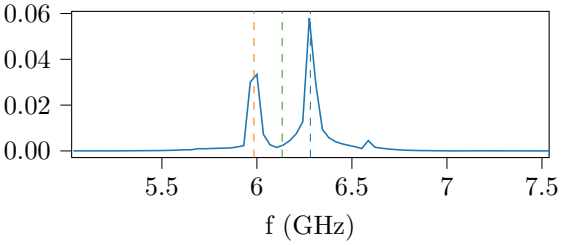

(e) Pulse length 29.0 ns

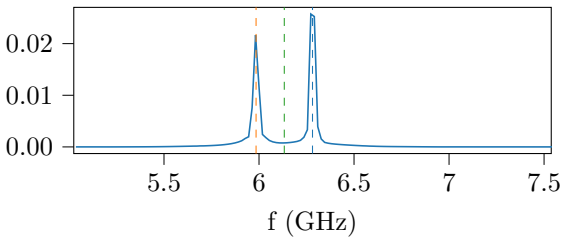

(f) Pulse length 55.0 ns

Figure 4.11: Pulse spectrum

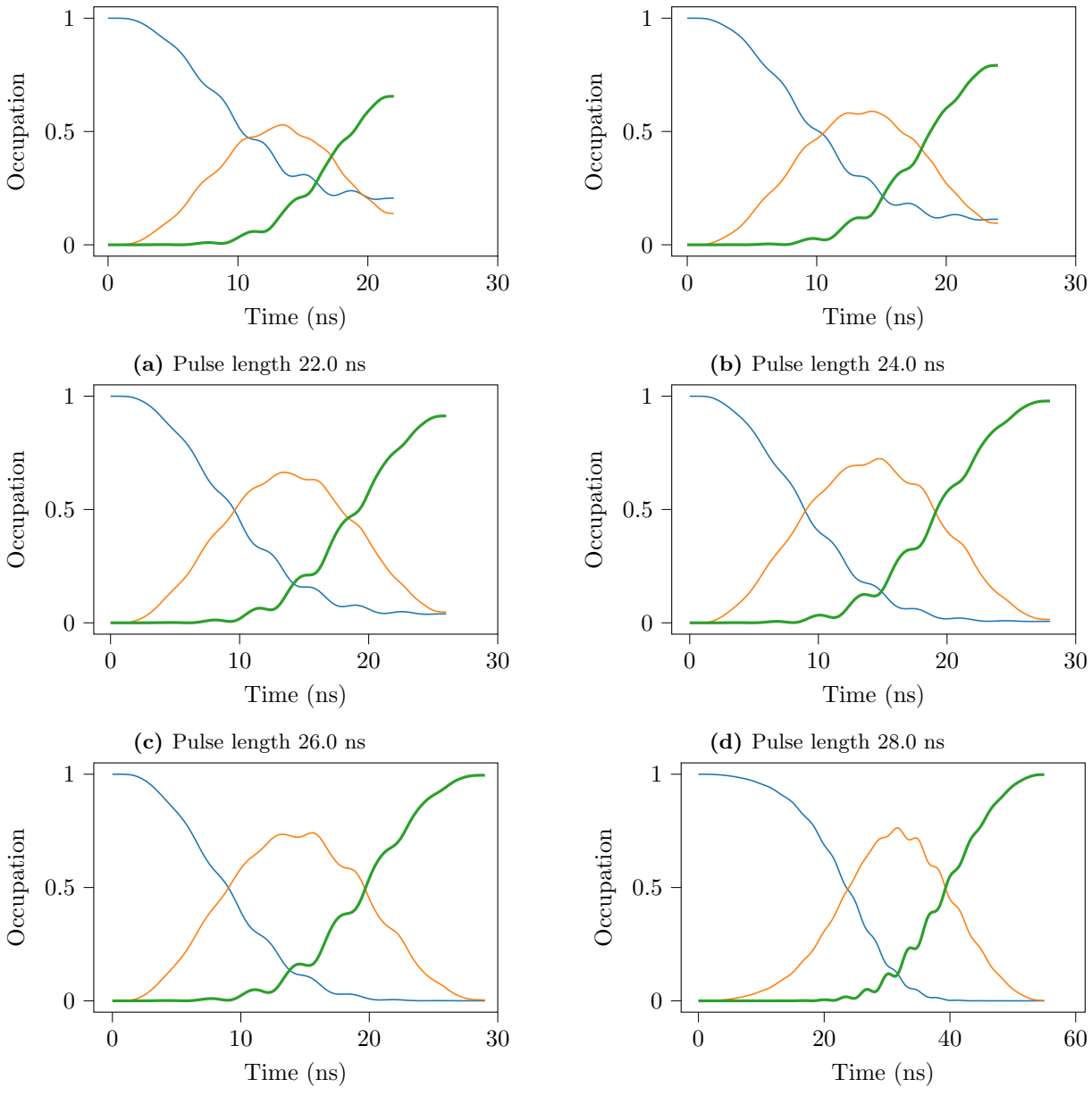

(a) Pulse length 22.0 ns

(b) Pulse length 24.0 ns

(c) Pulse length 26.0 ns

(d) Pulse length 28.0 ns

(e) Pulse length 29.0 ns

(f) Pulse length 55.0 ns

Figure 4.12: Energy level occupation over time for different lengths of optimized pulses.

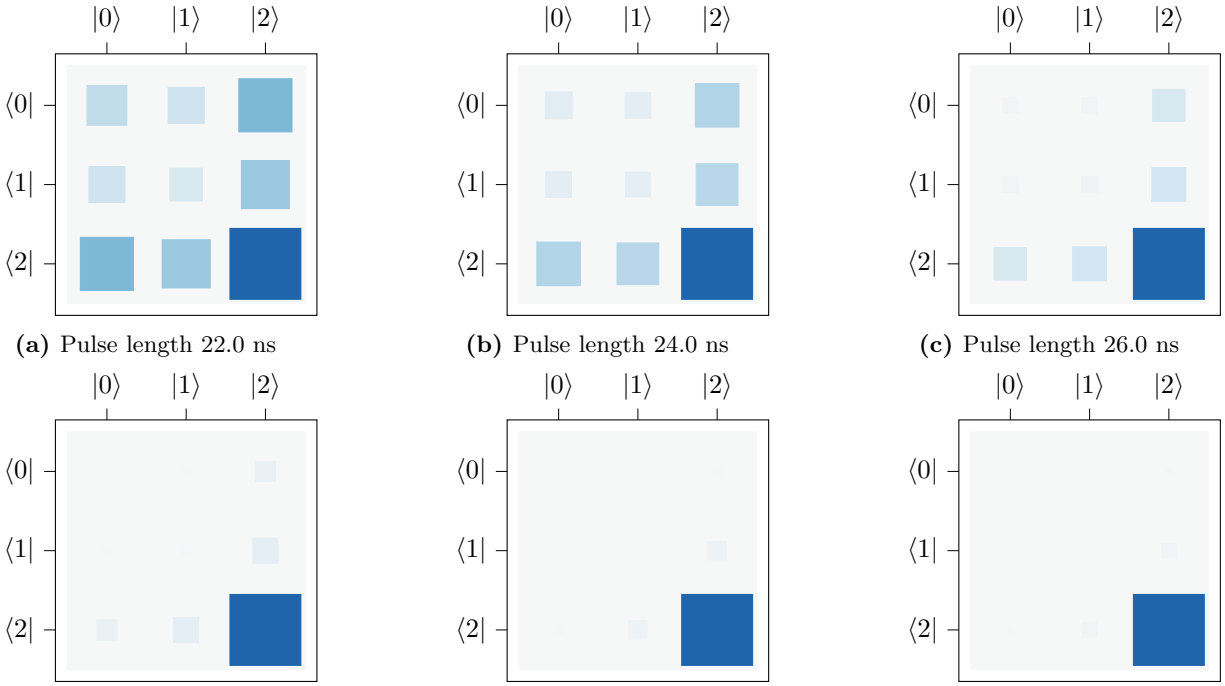

(a) Pulse length 22.0 ns **(b)** Pulse length 24.0 ns **(c)** Pulse length 26.0 ns

(d) Pulse length 28.0 ns **(e)** Pulse length 29.0 ns **(f)** Pulse length 55.0 ns

Figure 4.13: Hinton diagram of $|\psi(T)\rangle\langle\psi(T)|$

4.2.1 $|1\rangle_q |0\rangle_r \rightarrow |0\rangle_q |C_1\rangle_r$ state transfer

In this composite system it can be hard to see

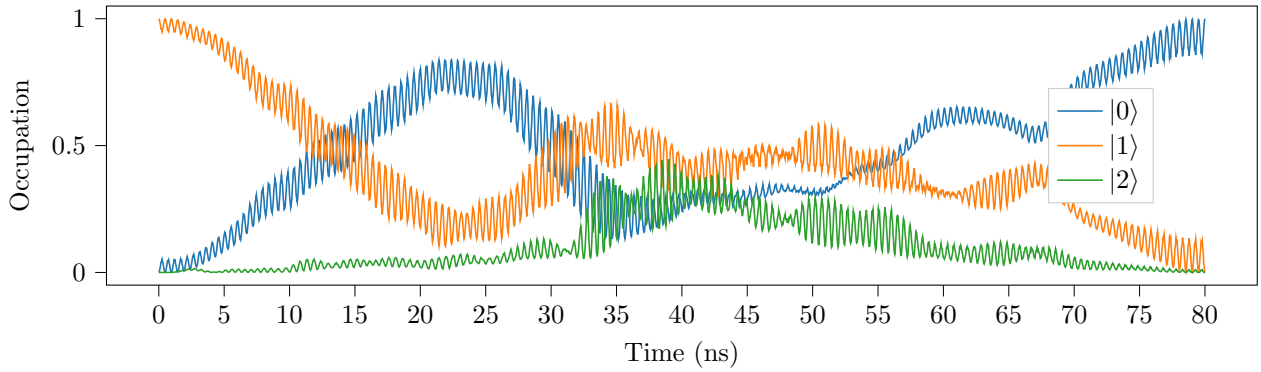

Figure 4.14: Occupation probability of the qubit over time.

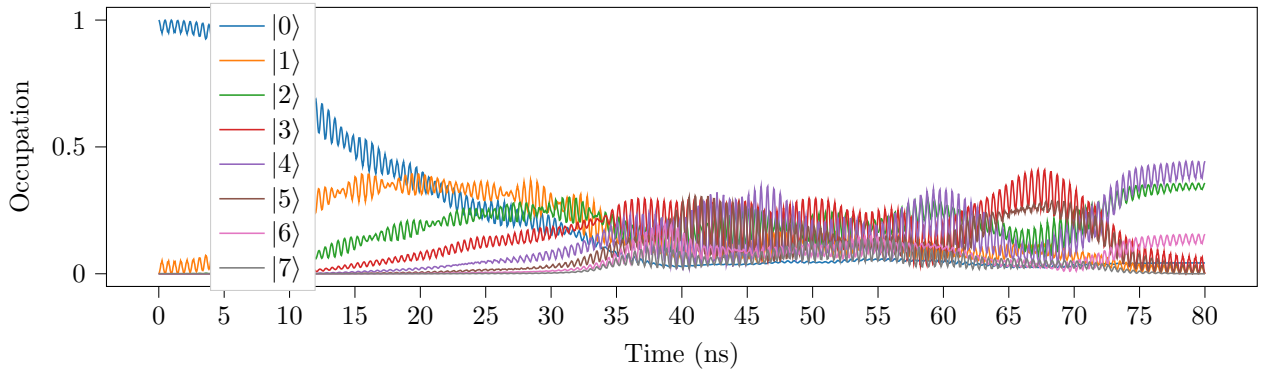

Figure 4.15: Occupation probability of the resonator over time.

Larger Hilbert space with the L=3 solution gives fidelities

5 Discussion

Reason to believe that 4 levels could be enough for the qubit

6 Conclusion

References

[1] A. C. Santos, The IBM Quantum Computer and the IBM Quantum Experience, *Revista Brasileira de Ensino de Física* **39**, no. 1 Sep. 2016, Sep. 2016, 00003 arXiv: 1610.06980, ISSN: 1806-1117. DOI: 10.1590/1806-9126-RBEF-2016-0155. [Online]. Available: http://arxiv.org/abs/1610.06980 (visited on 05/10/2019).

[2] J. Preskill, Quantum Computing in the NISQ era and beyond, *Quantum* **2** Aug. 2018, 79, Aug. 2018, 00180 arXiv: 1801.00862, ISSN: 2521-327X. DOI: 10.22331/q-2018-08-06-79. [Online]. Available: http://arxiv.org/abs/1801.00862 (visited on 02/28/2019).

[3] D. Gottesman, An Introduction to Quantum Error Correction and Fault-Tolerant Quantum Computation, *arXiv:0904.2557 [quant-ph]* Apr. 2009, Apr. 2009, 00221 arXiv: 0904.2557. [Online]. Available: http://arxiv.org/abs/0904.2557 (visited on 05/10/2019).

[4] Z. Leghtas, G. Kirchmair, B. Vlastakis, R. J. Schoelkopf, M. H. Devoret, and M. Mirrahimi, Hardware-Efficient Autonomous Quantum Memory Protection, *Physical Review Letters* **111**, no. 12 Sep. 2013, 120501, Sep. 2013, 00126. DOI: 10.1103/PhysRevLett.111.120501. [Online]. Available: https://link.aps.org/doi/10.1103/PhysRevLett.111.120501 (visited on 05/10/2019).

[5] M. Mirrahimi, Z. Leghtas, V. V. Albert, S. Touzard, R. J. Schoelkopf, L. Jiang, and M. H. Devoret, Dynamically protected cat-qubits: A new paradigm for universal quantum computation, *New Journal of Physics* **16**, no. 4 Apr. 2014, 045014, Apr. 2014, 00191 arXiv: 1312.2017, ISSN: 1367-2630. DOI: 10.1088/1367-2630/16/4/045014. [Online]. Available: http://arxiv.org/abs/1312.2017 (visited on 05/10/2019).

[6] N. Ofek, A. Petrenko, R. Heeres, P. Reinhold, Z. Leghtas, B. Vlastakis, Y. Liu, L. Frunzio, S. M. Girvin, L. Jiang, M. Mirrahimi, M. H. Devoret, and R. J. Schoelkopf, Extending the lifetime of a quantum bit with error correction in superconducting circuits, English, *Nature; London* **536**, no. 7617 Aug. 2016, 441–445, Aug. 2016, 00187, ISSN: 00280836. DOI: http://dx.doi.org.proxy.lib.chalmers.se/10.1038/nature18949. [Online]. Available: http://search.proquest.com/docview/1815378608/abstract/D91F00AED7CC42E9PQ/1 (visited on 01/23/2019).

[7] D. M. Reich, M. Ndong, and C. P. Koch, Monotonically convergent optimization in quantum control using Krotov's method, *The Journal of Chemical Physics* **136**, no. 10 Mar. 2012, 104103, Mar. 2012, 00103, ISSN: 0021-9606. DOI: 10.1063/1.3691827. [Online]. Available: https://aip.scitation.org/doi/10.1063/1.3691827 (visited on 04/29/2019).

[8] M. H. Goerz, D. Basilewitsch, F. Gago-Encinas, M. G. Krauss, K. P. Horn, D. M. Reich, and C. P. Koch, Krotov: A Python implementation of Krotov's method for quantum optimal control, *arXiv:1902.11284* 2019, 2019, 00000.

[9] *File:Bloch sphere.svg - Wikipedia*, 00000. [Online]. Available: https://en.wikipedia.org/wiki/File:Bloch_sphere.svg (visited on 05/22/2019).

[10] R. Fisher, "Optimal Control of Multi-Level Quantum Systems", 00000, Dissertation, Technische Universität München, München, 2010.

[11] D. d'Alessandro, *Introduction to quantum control and dynamics*. Chapman and Hall/CRC, 2007, 00626.

[12] J. R. Johansson, P. D. Nation, and F. Nori, QuTiP 2: A Python framework for the dynamics of open quantum systems, *Computer Physics Communications* **184**, no. 4 Apr. 2013, 1234–1240, Apr. 2013, 00646 arXiv: 1211.6518, ISSN: 00104655. DOI: 10.1016/j.cpc.2012.11.019. [Online]. Available: http://arxiv.org/abs/1211.6518 (visited on 05/28/2019).